



OPEN ACCESS

EDITED BY

Latika Gupta,
Royal Wolverhampton Hospitals NHS
Trust, United Kingdom

REVIEWED BY

Naveen R,
Sanjay Gandhi Postgraduate Institute
of Medical Sciences, India
Didem Saygin,
University of Pittsburgh, United States

*CORRESPONDENCE

Masataka Kuwana
✉ kuwanam@nms.ac.jp

SPECIALTY SECTION

This article was submitted to
Rheumatology,
a section of the journal
Frontiers in Medicine

RECEIVED 11 October 2022

ACCEPTED 12 December 2022

PUBLISHED 04 January 2023

CITATION

Kadota H, Gono T, Kunugi S, Ota Y,
Takeno M, Seike M, Shimizu A and
Kuwana M (2023) Tertiary lymphoid
structures in the primary tumor site
of patients with cancer-associated
myositis: A case–control study.
Front. Med. 9:1066858.
doi: 10.3389/fmed.2022.1066858

COPYRIGHT

© 2023 Kadota, Gono, Kunugi, Ota,
Takeno, Seike, Shimizu and Kuwana.
This is an open-access article
distributed under the terms of the
[Creative Commons Attribution License
\(CC BY\)](https://creativecommons.org/licenses/by/4.0/). The use, distribution or
reproduction in other forums is
permitted, provided the original
author(s) and the copyright owner(s)
are credited and that the original
publication in this journal is cited, in
accordance with accepted academic
practice. No use, distribution or
reproduction is permitted which does
not comply with these terms.

Tertiary lymphoid structures in the primary tumor site of patients with cancer-associated myositis: A case–control study

Hiroko Kadota¹, Takahisa Gono^{1,2}, Shinobu Kunugi³,
Yuko Ota^{1,2}, Mitsuhiro Takeno^{1,4}, Masahiro Seike⁵,
Akira Shimizu³ and Masataka Kuwana^{1,2*}

¹Department of Allergy and Rheumatology, Graduate School of Medicine, Nippon Medical School, Tokyo, Japan, ²Scleroderma/Myositis Center of Excellence, Nippon Medical School Hospital, Tokyo, Japan, ³Department of Analytic Human Pathology, Graduate School of Medicine, Nippon Medical School, Tokyo, Japan, ⁴Department of Allergy and Rheumatology, Nippon Medical School Musashi Kosugi Hospital, Kawasaki, Japan, ⁵Department of Pulmonary Medicine and Oncology, Graduate School of Medicine, Nippon Medical School, Tokyo, Japan

Objective: To investigate histologic features of immunological components in the primary tumor site of patients with cancer-associated myositis (CAM) by focusing on tumor-infiltrating lymphocytes (TILs) and tertiary lymphoid structures (TLSs), which play major roles in antitumor immunity.

Methods: Cancer-associated myositis patients were selected from the single-center idiopathic inflammatory myopathy cohort based on the availability of primary tumor specimens obtained before the introduction of immunomodulatory agents. Control cancer subjects without CAM were selected from the cancer tissue repository at a ratio of 1:2 matched for demographics and cancer characteristics of CAM cases. A series of immunohistochemical analyses was conducted using sequential tumor sections. TLS was defined as an ectopic lymphoid-like structure composed of DC-LAMP⁺ mature dendritic cells, CD23⁺ follicular dendritic cells (FDCs) and PNA⁺ high endothelial venules. TLS distribution was classified into the tumor center, invasive margin, and peritumoral area.

Results: Six CAM patients and 12 matched non-CAM controls were eligible for the study. There was no apparent difference in the density or distribution of TILs between the groups. TLSs were found in 3 CAM patients (50%) and 4 non-CAM controls (33%). TLSs were exclusively located at the tumor center or invasive margin in CAM cases but were mainly found in the peritumoral area in non-CAM controls. FDCs and class-switched B cells colocalized with follicular

helper T cells were abundantly found in the germinal center-like area of TLSs from CAM patients compared with those from non-CAM controls.

Conclusion: The adaptive immune response within TLSs in the primary tumor site might contribute to the pathogenic process of CAM.

KEYWORDS

B cells, cancer, dermatomyositis, follicular dendritic cells, follicular helper T cell, myositis, tertiary lymphoid structure, tumor-infiltrating lymphocyte

Introduction

Idiopathic inflammatory myopathies (IIMs) are a group of conditions that affect skeletal muscles as well as extramuscular systems, such as skin, joints, heart, and lungs (1). The pathophysiology of IIMs remains uncertain, but it involves autoimmune responses characterized by production of a series of autoantibodies and activation of autoreactive T cells (2, 3). Adult patients with IIMs, including polymyositis (PM) and dermatomyositis (DM), have a higher risk for developing cancer than the general population (4, 5). Cancer-associated myositis (CAM) is defined as IIMs developing within a few years before or after the diagnosis of cancer (6, 7). CAM is considered a paraneoplastic syndrome because of the temporal relationship of the occurrence of these conditions. This is supported by the improvement of IIMs in several cases after resection of cancer without immunosuppressive therapy (8). It has been proposed that antitumor immune responses play a role in developing CAM, but few data are available on the adaptive immune response in the primary tumor site in CAM patients.

Accumulating lines of evidence have demonstrated the remarkable efficacy of immune checkpoint inhibitors on a variety of cancer types (9), indicating the indispensable role of adaptive immune responses against tumor cells in protection from cancer. Tumor-infiltrating lymphocytes (TILs) are a primary driver of adaptive immune responses against cancer, and the distribution, clustering, and interplay of their components are critical for eliciting effective antitumor immune response (10). TILs are located in the cancer stroma as aggregates or within tertiary lymphoid structures (TLSs), which are ectopic secondary lymphoid formations in the non-lymphoid tissue (11). TLSs are found not only in cancer lesions but also in chronically inflamed tissue in patients with various autoimmune diseases, allograft rejection, and infection, indicating a primary role in eliciting and maintaining acquired immune responses against tumor antigens, autoantigens, alloantigens, and foreign antigens (12). In fact, the appearance of TLSs in cancer lesions is associated with better overall survival in patients with various types of cancer (13, 14). In this case-control study, histologic features of the primary tumor site of CAM patients were compared with those of non-CAM cancer

controls matched for demographic and cancer characteristics, focusing on TILs and TLSs.

Materials and methods

Subjects

In this case-control study, patients with CAM were selected from the IIM database of the Scleroderma/Myositis Center of Excellence at Nippon Medical School Hospital, established in July 2014, based on the following criteria: (i) fulfillment of the 2017 European League against Rheumatism (EULAR)/American College of Rheumatology (ACR) classification criteria for IIMs (15); (ii) age at diagnosis ≥ 18 years; (iii) development of IIMs within 3 years before or after the diagnosis of cancer (6); (iv) resection of the primary tumor before treatment with any immunomodulatory agents, including glucocorticoids, immunosuppressants, cytotoxic anticancer agents, molecular targeted agents, and immune checkpoint inhibitors; and v) availability of the resected primary tumor tissue for histologic evaluation. Subclassification of the IIM patients into DM, amyopathic DM (ADM), immune-mediated necrotizing myopathy (IMNM) or PM, and inclusion body myositis was made according to the EULAR/ACR classification criteria (15). Control non-CAM cancer subjects were selected from the cancer tissue repository of the Nippon Medical School Hospital (Clinical Rebiopsy Bank), which collects surgical specimens of primary tumor lesions from patients with lung, stomach, colon, breast, or ovarian cancer (16), and matched for age at cancer diagnosis (± 10 years), gender, tumor type, tumor nodule metastasis (TNM) classification of cancer, and tumor histology with CAM cases in a 1:2 ratio. All non-CAM controls had no history of any autoimmune diseases listed by the American Association of Autoimmune-Related Diseases¹ and no record of preoperative adjuvant chemotherapy. This study was approved by the Institutional Review Board of Nippon Medical School Hospital

¹ <https://www.aarda.org/diseaselist/>

(approval number 28-12-680), and written informed consent was obtained from all subjects.

Clinical data

Standard demographic and clinical information of CAM patients was retrieved from the IIM database. Information regarding cancer was additionally obtained by a retrospective chart review and included age at diagnosis of CAM, age at surgery for cancer, sex, subclassification of IIMs, tumor type, TNM classification (17), tumor histology, treatment for IIMs and cancer, and outcomes of IIMs and cancer at the latest visit. Myositis-specific autoantibodies (MSAs) and myositis-associated autoantibodies (MAAs) were identified by immunoprecipitation combined with immunoblots (18), RNA immunoprecipitation assay (19), and a commercially available enzyme-linked immunosorbent assay kit (20).

Tissue staining

Paraffin-embedded 4 μm -thick sections were prepared from tumor blocks containing the boundary between cancer and non-cancer areas confirmed by a skilled pathologist (SK). Then, the sections were deparaffinized in xylene, rehydrated with a graded series of ethanol solutions, and subjected to hematoxylin and eosin (HE) staining. For immunohistochemical staining, the sections were used for antigen retrieval, treated with absolute methanol containing 0.3% hydrogen peroxidase for 10 min to block endogenous peroxidase activity, and incubated for 1 h at room temperature or overnight at 4°C with one of the primary antibodies, including anti-CD3, anti-CD4, anti-CD8, anti-CD20, anti-dendritic cell lysosome-associated membrane glycoprotein (DC-LAMP), anti-CD23, anti-peripheral node addressin (PNAd), anti-CD138, anti-B-cell lymphoma 6 (BCL6), and anti-activation-induced cytidine deaminase (AID) antibodies (21). **Supplementary Table 1** summarizes a list of the primary antibodies and antigen retrieval methods used for immunohistochemical analysis. The sections were subsequently incubated with a universal polymer containing peroxidase-conjugated goat anti-IgG Fab' (Histofine® Simple Stain PO(M) kit; Nichirei, Tokyo, Japan) (22), and the signals were visualized using 3,3'-diaminobenzidine (DAB). For the detection of PNAd, biotinylated anti-rat IgM antibodies (Abcam: Cambridge, UK) were employed, followed by incubation with peroxidase-labeled streptavidin. Mouse IgG1 or rabbit immunoglobulin (Dako Denmark A/S, Glostrup, Denmark) was used as a negative control. After counterstaining with hematoxylin, these slides were mounted and examined with an optical microscope (IX-81 inverted microscopes: Olympus, Tokyo, Japan), and images were recorded using the virtual slide system (SCN400F: Leica, Wetzlar, Germany).

Immunofluorescent double staining was performed according to published methods (23). Briefly, formalin-fixed and paraffin-embedded sections were deparaffinized, rehydrated, pretreated in Tris/ethylenediaminetetraacetic acid buffer (pH 9.0), and subjected to microwave treatment for 20 min. Non-specific binding sites were blocked with phosphate-buffered saline containing 5% bovine serum albumin for 60 min at room temperature, followed by incubation with different combinations of primary antibodies, including anti-CD4, anti-BCL6, and anti-AID antibodies, overnight at 4°C (**Supplementary Table 1**). The secondary antibodies used included goat anti-rabbit IgG-Alexa 488 and goat anti-mouse IgG-Alexa 568 (Abcam). Nuclei were counterstained with 4',6-diamidino-2'-phenylindole dihydrochloride (DAPI; Thermo Fisher Scientific, Waltham, MA, USA). These slides were examined with a confocal laser fluorescence microscope (LSM 800 with Airyscan: ZEISS, Oberkochen, Germany), and images were recorded using a microscope digital camera (DP74; Olympus) with CellSens Dimension 2.3 software (Olympus).

Histologic assessment

Slide images stored in the virtual slide system were used for the computerized quantitative assessment with the bioimage analysis software QuPath² (24). After areas with crush, necrosis, hyalinization, non-specific staining, and artifacts generated during specimen preparation were excluded from the overall assessment (25), we defined the tissue region to be analyzed (simple tissue detection). The malignant tumor area was identified by a pathologist (SK) and was divided into three regions: invasive margin (IM), a 1 mm-wide area centered on the boundary between the cancer and non-cancer areas; central tumor (CT), the cancer area inside the IM; and peritumor (PT), the non-cancer area outside the IM (25). Next, all the cells in the area of interest were detected by using a built-in cell segmentation algorithm (cell detection), followed by classification of cell types and the presence or absence of staining (detection classifier). Finally, the number of stained immune cells (CD4/CD8/CD20) in the selected region was counted, and the density (cells/mm²) and the CD4/CD8 ratio were calculated. TILs were defined as lymphocytes infiltrated within the CT and IM areas (25).

TLSs were defined as an ectopic lymphoid-like structure detected in sequential sections that satisfied all of the following characteristics: (i) adjacent CD3⁺ T-cell and CD20⁺ B-cell areas; (ii) PNAd⁺ high endothelial venule (HEV) in and around the follicular structure; (iii) CD23⁺ follicular dendritic cells (FDCs) in the B-cell area; and (iv) DC-LAMP⁺ mature dendritic cells (DCs) in the T-cell area (26). TLSs with clear boundaries of the T-cell and B-cell areas were regarded as

² <https://qupath.github.io>

well-organized TLSs (27). TLS-like structures were defined as lymphocyte aggregation areas of $\geq 7,000 \mu\text{m}^2$ that did not meet the criteria for TLS (28). In addition, TLS-like structures were further classified into PNA⁺, CD23⁺, and DC-LAMP⁺ TLS-like structures based on satisfaction of a criterion for PNA⁺ HEV, CD23⁺ FDCs, or DC-LAMP⁺ mature DCs, respectively. The numbers of TLSs and TLS-like structures were counted in whole sections from individual subjects. We also assessed the density (cells/mm²), distribution (IM/CT/PT), maturity (well-organized/total TLS [%]), and mean diameter (mm²) of TLSs in individual subjects. The density of CD4⁺ T cells, CD8⁺ T cells, CD20⁺ B cells, AID⁺ cells, CD23⁺ FDCs, PNA⁺ HEV, CD138⁺ plasma cells, and CD4⁺BCL6⁺ T follicular helper (Tfh) cells within the TLS was also evaluated and is shown in cells/mm² except for CD23⁺ FDCs, which are shown as percentages.

Statistical analysis

Continuous variables are shown as the mean \pm standard deviation (SD) or median and range, as appropriate. A two-sided t test or Mann–Whitney U test was used to compare parametric and non-parametric variables, respectively. All statistical analyses were performed using the software program R (R version 4.1.3).

Results

Patient characteristics

Of 160 patients registered in the IIM database, 35 patients were classified as having CAM. The primary tumor specimen

was available in 9 patients. After exclusion of 3 patients who received immunomodulatory agents before surgery, 6 patients with CAM were eligible for this study (Supplementary Figure 1). Twelve cancer patients without CAM who were matched for age at cancer diagnosis, sex, tumor type, TNM classification, and tumor histology were selected from the Clinical Rebiopsy Bank as non-CAM controls. The clinical characteristics of the 6 patients with CAM are shown in Table 1. All but one had classic DM or ADM, and the remaining patient was diagnosed with IMNM. The mean age at the time of diagnosis of IIM was 66.0 ± 8.7 years, and the median period from the diagnosis of IIM to cancer resection surgery was -3.5 months (range, -31 to 0). Two patients were positive for anti-TIF1- γ antibody, and anti-PL-12, anti-NXP2, and anti-SRP antibodies were positive in one patient each. The primary cancer sites included the stomach in 2 patients and the breast, lung, colorectum, and ovary in one patient each. The histological type was adenocarcinoma in all patients. Only one died of colorectal cancer 7 months after cancer diagnosis. The clinical characteristics of the 12 non-CAM controls are shown in Supplementary Table 2.

TILs in CAM and non-CAM controls

The density of CD4⁺ T cells, CD8⁺ T cells, and CD20⁺ B cells in the CT and IM areas of the cancer tissue was similar between the 6 CAM patients and 12 non-CAM patients (Figure 1). CD4⁺ T cells in the CT and IM areas tended to be increased in CAM patients compared with non-CAM patients ($P = 0.13$ and 0.37 , respectively), but the difference did not reach statistical significance, probably due to the small number of patients and a large variation among subjects.

TABLE 1 Clinical characteristics of 6 patients with CAM.

Characteristics	CAM #1	CAM #2	CAM #3	CAM #4	CAM #5	CAM #6
Age at IIM diagnosis, years	69	65	62	77	73	50
Age at cancer resection surgery, years	69	64	62	74	73	49
Gender	Male	Female	Female	Male	Female	Female
IIM sub-classification	ADM	ADM	Classic DM	Classic DM	IMNM	Classic DM
MSAs/MAAs	Anti-PL-12	Negative	Anti-TIF1- γ	Anti-NXP2	Anti-SRP	Anti-TIF1- γ
Months from IIM diagnosis to surgery	0	-18	0	-31	-1	-6
Primary cancer site	Stomach	Stomach	Breast	Lung	Colorectum	Ovary
Cancer histological type	Adeno-carcinoma	Adeno-carcinoma	Adeno-carcinoma	Adeno-carcinoma	Adeno-carcinoma	Adeno-carcinoma
TNM classification	pT1b2 (SM2)	pT1N0M0	pT1N1aM0	pT2aN0M0	pT3aN0M0	pT3cNxM1b
Months from cancer diagnosis to last observation	186	76	157	49	7	23
Outcome at last observation	Alive	Alive	Alive	Alive	Dead	Alive

CAM, cancer-associated myositis; ADM, amyopathic dermatomyositis; DM, dermatomyositis; IMNM, immune-mediated necrotizing myopathy; MSA, myositis-specific antibody; MAA, myositis-associated antibody; TIF1- γ , transcriptional intermediary factor 1- γ ; NXP2, nuclear matrix protein 2; SRP, anti-signal recognition particle; TNM: tumor-node-metastasis.

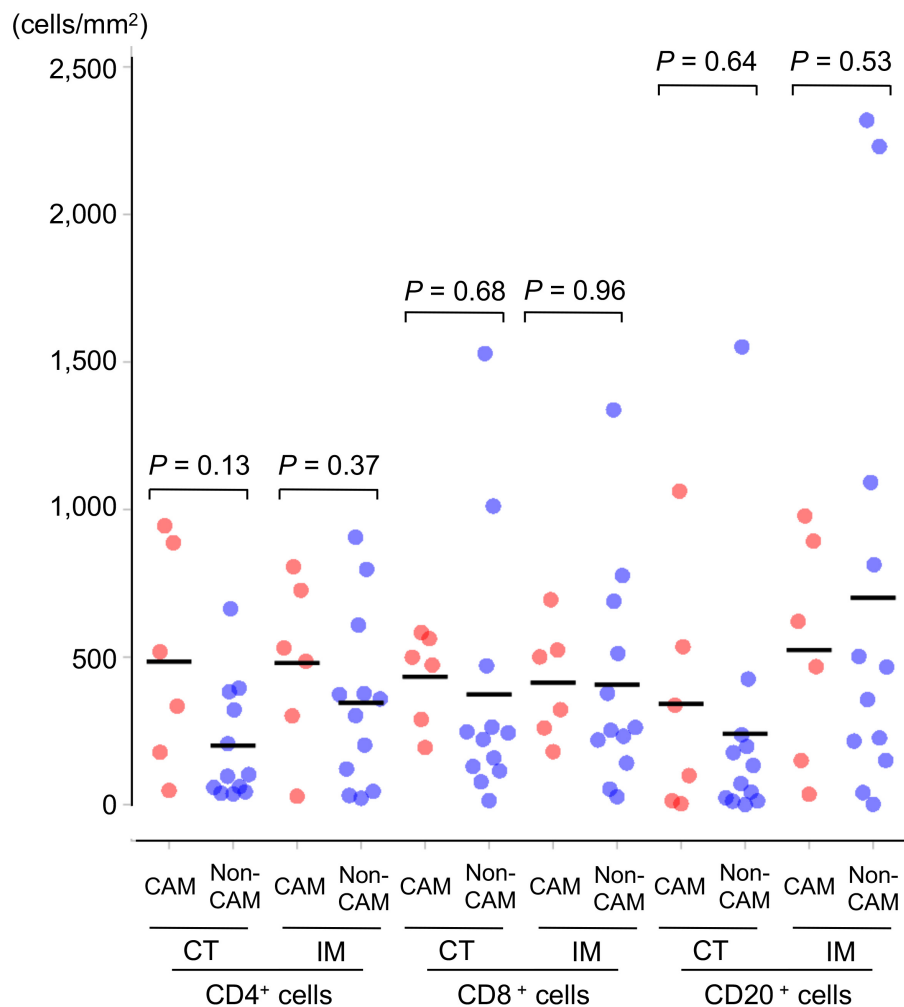


FIGURE 1

Density of TILs in 6 CAM patients and 12 non-CAM controls. The density of tumor-infiltrating CD4⁺ T cells, CD8⁺ T cells, and CD20⁺ B cells in the CT and IM areas of the cancer tissue was analyzed by computerized quantitative assessment using the bioimage analysis software QuPath. Horizontal lines denote the mean. CAM, cancer-associated myositis; TILs, tumor-infiltrating lymphocytes; CT, central tumor; IM, invasive margin.

TLS in CAM and non-CAM controls

Representative histological findings of TLSs found in CAM #2 are shown in [Figure 2](#). A secondary lymphoid-like formation was easily identified by HE staining. A typical histologic characteristic of TLSs is a lymphoid follicle composed of an inner zone of CD20⁺ B cells (B-cell zone) and surrounding CD3⁺ T cells, mainly consisting of CD4⁺ T cells (T-cell zone). PNAd⁺ HEV and DC-LAMP⁺ mature DCs were predominantly localized in the T-cell zone. A germinal center (GC)-like structure, which was defined by the presence of CD23⁺ FDCs, formed a tight network in the B-cell zone within the follicle-like structure. Moreover, subgroups of lymphocytes in the GC-like structure expressed BCL6 or AID. CD138⁺ plasma cells were detected around TLSs in the stroma of the tumor tissue. Typical TLSs were detected in the tumor tissue of 3

(50%) of 6 CAM patients and 4 (33%) of 12 non-CAM controls. The number of TLSs and TLS-like structures in CAM patients and non-CAM controls is shown in [Figure 3](#). There was a trend toward increased TLSs and TLS-like structures, especially CD23⁺ TLS-like structures, in CAM patients compared with non-CAM controls, but there was no statistically significant difference.

To further investigate the detailed histological features of TLSs, a total of 20 TLSs detected in 3 CAM patients (two with gastric cancer and one with breast cancer) were compared with a total of 11 TLSs detected in 3 non-CAM controls matched for cancer type ([Table 2](#)). The total number and density of TLSs were numerically higher in CAM patients than in non-CAM controls. Low-magnification HE staining and CD20 staining of tumor sections in 3 CAM patients and 3 non-CAM controls revealed that TLSs were located exclusively in the CT or IM area

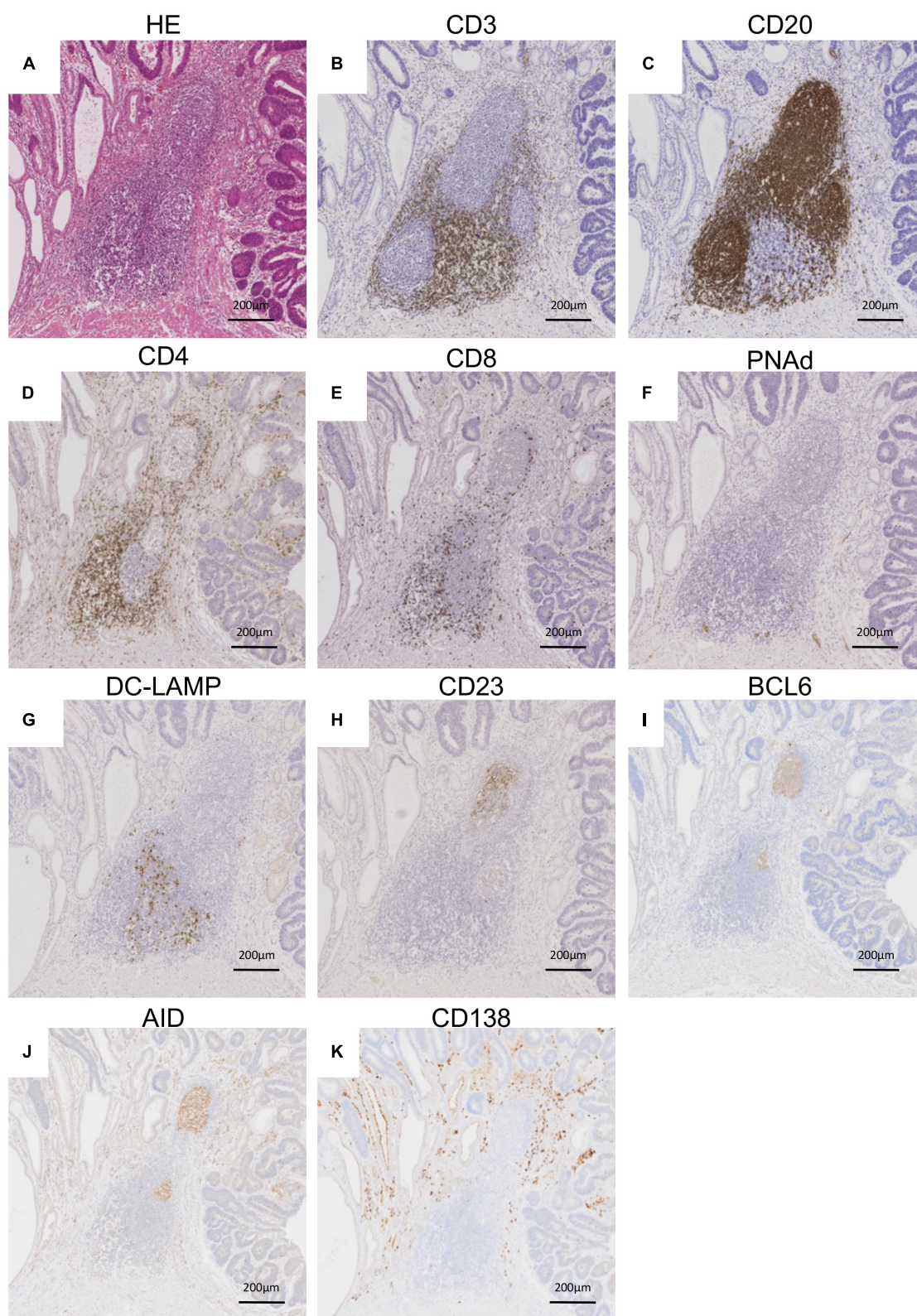


FIGURE 2

Representative histological features of TLS. Serial sections of the stomach cancer tissue from a representative CAM patient (CAM #2) were subjected to HE staining (A) and immunohistochemical staining for CD3 (B), CD20 (C), CD4 (D), CD8 (E), PNAf (F), DC-LAMP (G), CD23 (H), BCL6 (I), AID (J), and CD138 (K). Scale bar = 200 µm. TLSs, tertiary lymphoid structures; HE, hematoxylin and eosin; PNAf, peripheral node addressin; DC-LAMP, dendritic cell lysosomal associated membrane glycoprotein; BCL6, B-cell lymphoma 6; AID, activation induced deaminase.

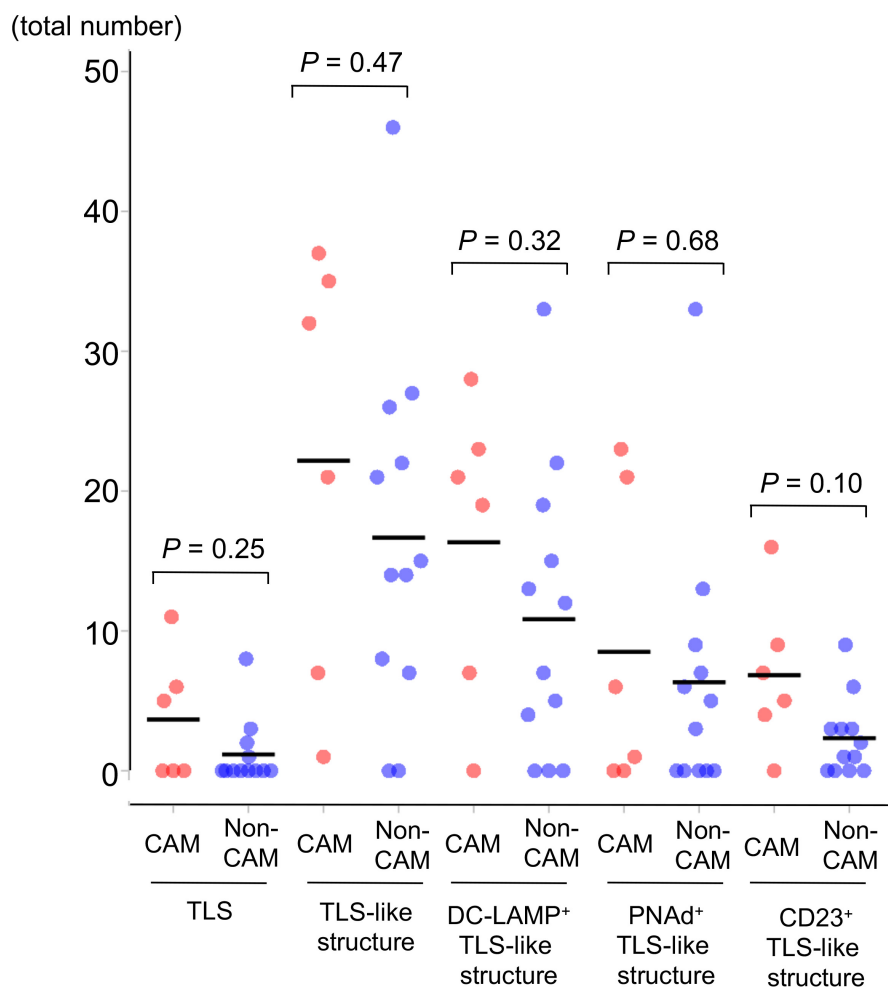


FIGURE 3

The number of TLSs and TLS-like structures in 6 CAM patients and 12 non-CAM controls. The number of TLSs, TLS-like structures, DC-LAMP⁺ TLS-like structures, PNAAd⁺ TLS-like structures, and CD23⁺ TLS-like structures was analyzed by computerized quantitative assessment using the bioimage analysis software QuPath. The horizontal lines denote the mean. TLSs, tertiary lymphoid structures; TL, tumor-infiltrating lymphocyte; CAM, cancer-associated myositis; DC-LAMP, dendritic cell lysosomal associated membrane glycoprotein; PNAAd, peripheral node addressin.

TABLE 2 Histopathological features of TLSs in 3 CAM patients and 3 non-CAM controls.

Features	CAM			Non-CAM		
	#1	#2	#3	#1	#2	#3
Primary cancer site	Stomach	Stomach	Breast	Stomach	Stomach	Breast
Total number of TLSs	6	5	11	8	2	1
Density (/mm ²)	0.049	0.047	0.025	0.029	0.014	0.0030
Distribution						
CT	3	0	0	0	0	0
IM	3	5	11	3	0	1
PT	0	0	0	5	2	0
Maturity (%)*	0	80	0	38	0	0
Size of TLSs (mm ²)	0.10 ± 0.04	0.34 ± 0.13	0.34 ± 0.27	0.42 ± 0.34	0.10 ± 0.02	0.16

*Maturity is expressed as the proportion (%) of well-organized TLSs in total TLSs.

TLS, tertiary lymphoid structures; CAM, cancer-associated myositis; CT, central tumor; IM, invasive margin; PT, peritumor.

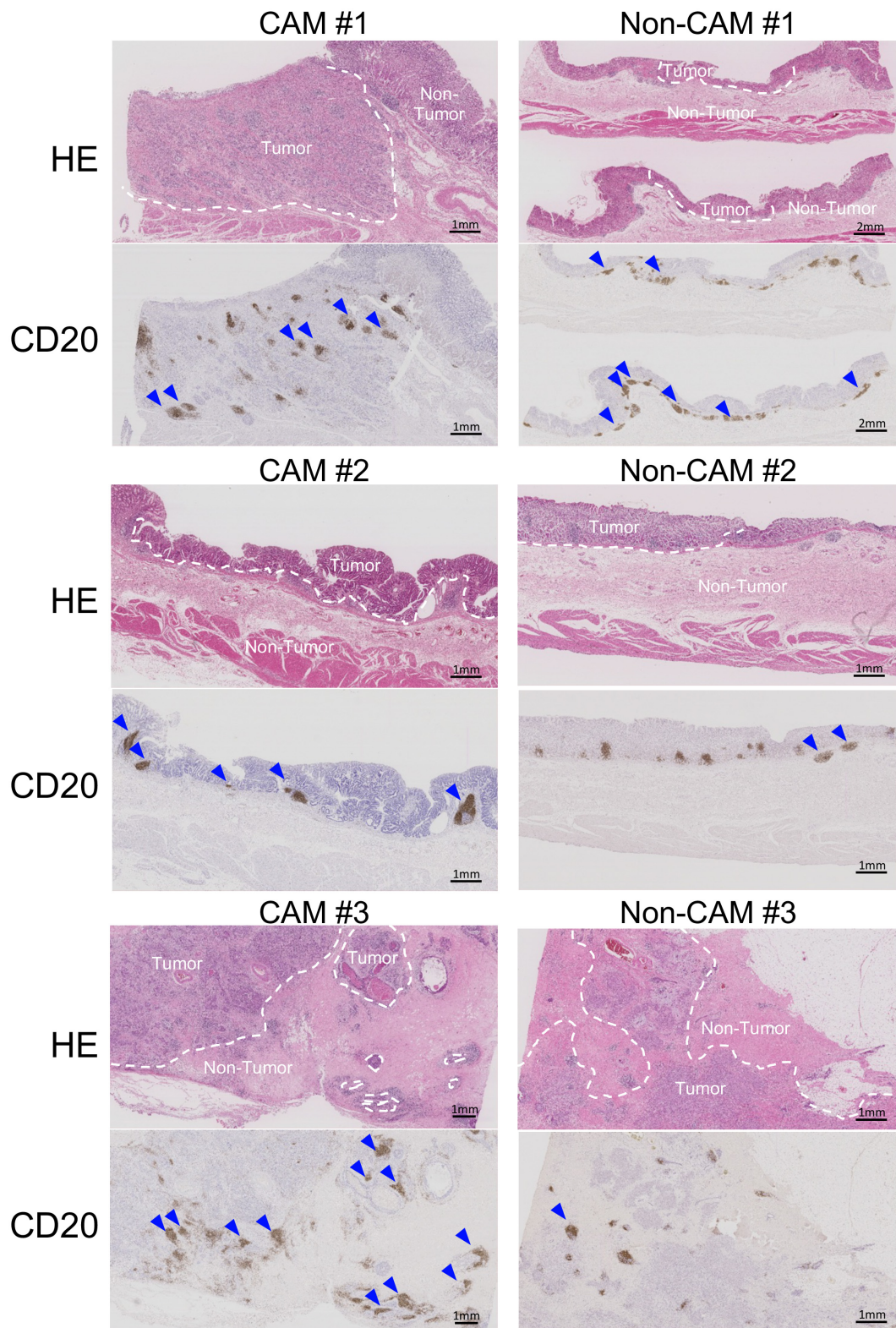
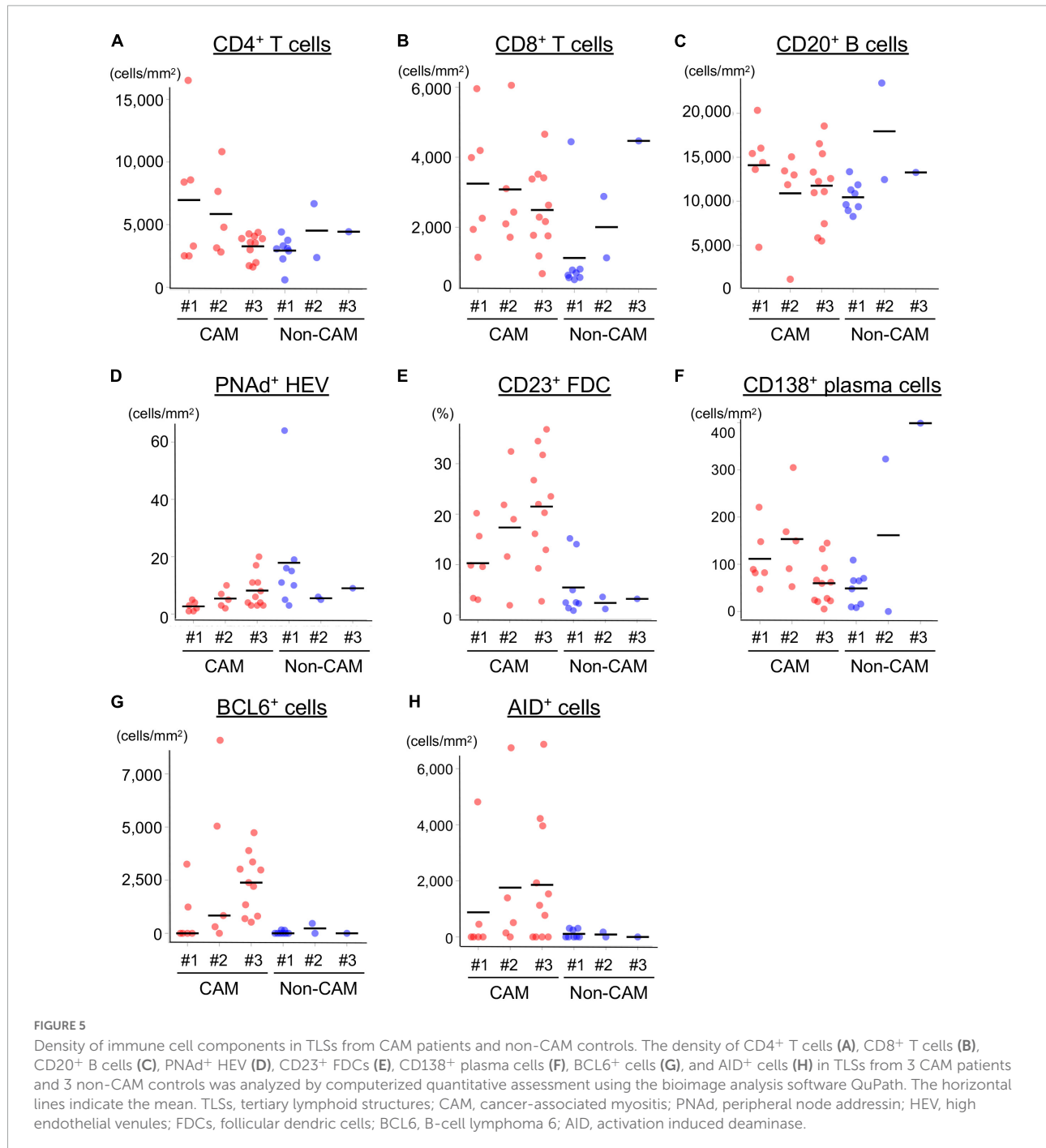


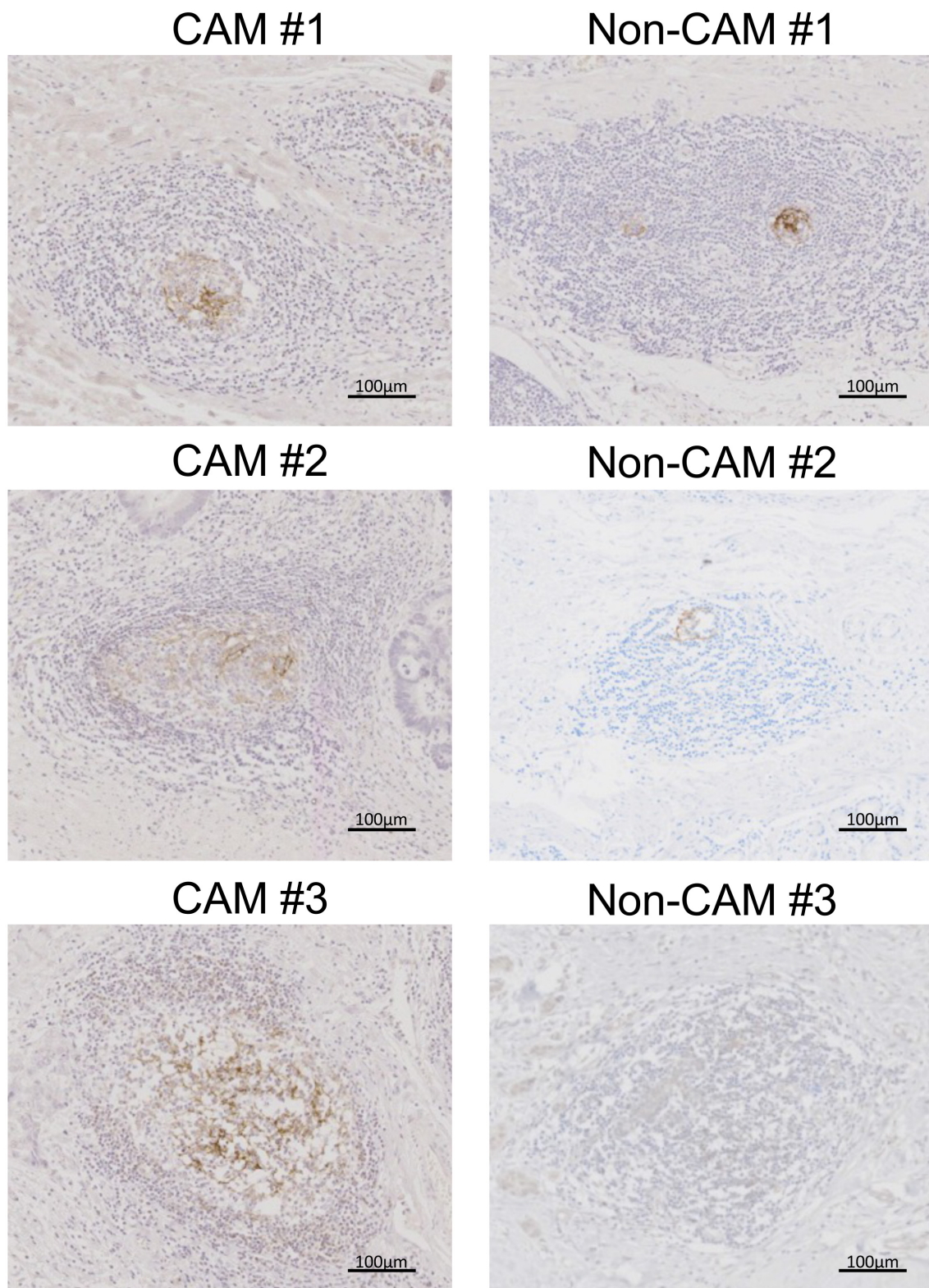
FIGURE 4
 Low-magnification images of TLs in 3 CAM patients and 3 non-CAM controls. HE staining and CD20 immunostaining were conducted in sequential tumor sections in 3 CAM patients (CAM #1-#3) and 3 non-CAM controls (non-CAM #1-#3). Broken lines in HE staining indicate the border between the tumor and non-tumor lesions, while blue arrows show TLs with CD20⁺ B-cell aggregates. Scale bar = 1mm (2 μm in non-CAM #1) CAM, cancer-associated myositis; HE, hematoxylin and eosin.

in CAM patients, while TLSs were located mainly in the PT area in non-CAM controls (Figure 4). The maturity and size of TLSs were comparable between the groups.

The cell densities of CD4⁺ T cells, CD8⁺ T cells, CD20⁺ B cells, PNA⁺ HEV, CD23⁺ FDCs, CD138⁺ plasma cells, BCL6⁺ cells, and AID⁺ cells were evaluated in 20 TLSs from 3 CAM patients and 11 TLSs from non-CAM controls (Figure 5). We did not evaluate naïve and memory B cells separately since it has been reported that B cells in cancer tissues are mainly

composed of memory B cells (29). Statistical analysis was not performed since the number of TLSs used for comparison varied among patients, resulting in the potential influence of data from particular patients on the overall results. There was no explicit difference in the density of CD4⁺, CD8⁺, and CD20⁺ cells; PNA⁺ HEV; or CD138⁺ plasma cells between TLSs derived from CAM patients and those from non-CAM controls. On the other hand, the densities of CD23⁺ FDCs, BCL6⁺ cells, and AID⁺ cells in TLSs were numerically



**FIGURE 6**

CD23⁺ FDCs in TLSs from CAM patients and non-CAM controls. CD23 immunostaining was conducted in representative TLSs from 3 CAM patients (CAM #1-#3) and 3 non-CAM controls (non-CAM #1-#3). Scale bar = 100 μ m. FDCs, follicular dendritic cells; TLSs, tertiary lymphoid structures; CAM, cancer-associated myositis.

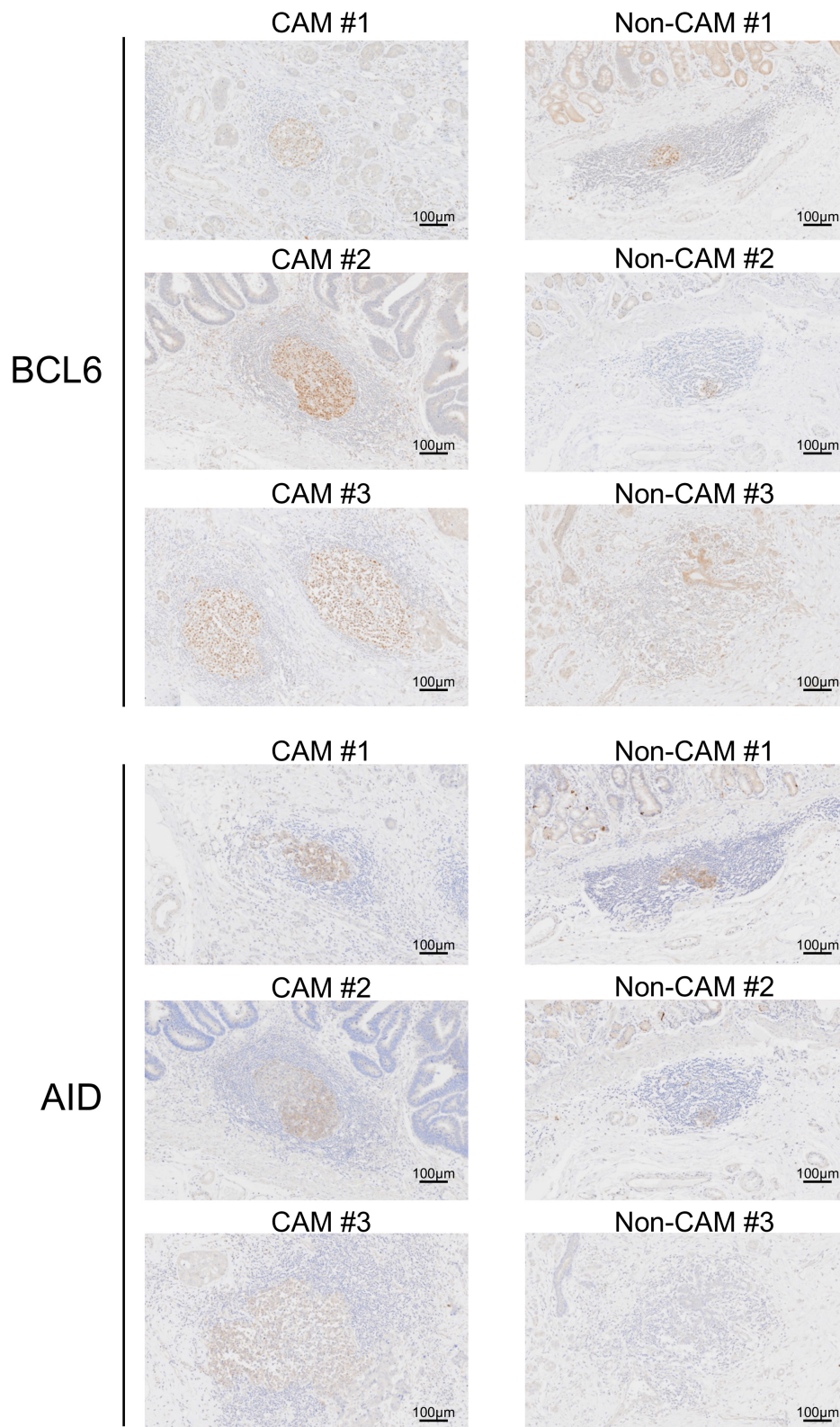


FIGURE 7

BCL6⁺ cells and AID⁺ cells in TLSs from CAM patients and non-CAM controls. Immunostaining for BCL6 or AID was conducted in representative TLSs from 3 CAM patients (CAM #1-#3) and 3 non-CAM controls (non-CAM #1-#3). Scale bar = 100 μm. CAM, cancer-associated myositis; TLSs, tertiary lymphoid structures; BCL6, B-cell lymphoma 6; AID, activation induced deaminase.

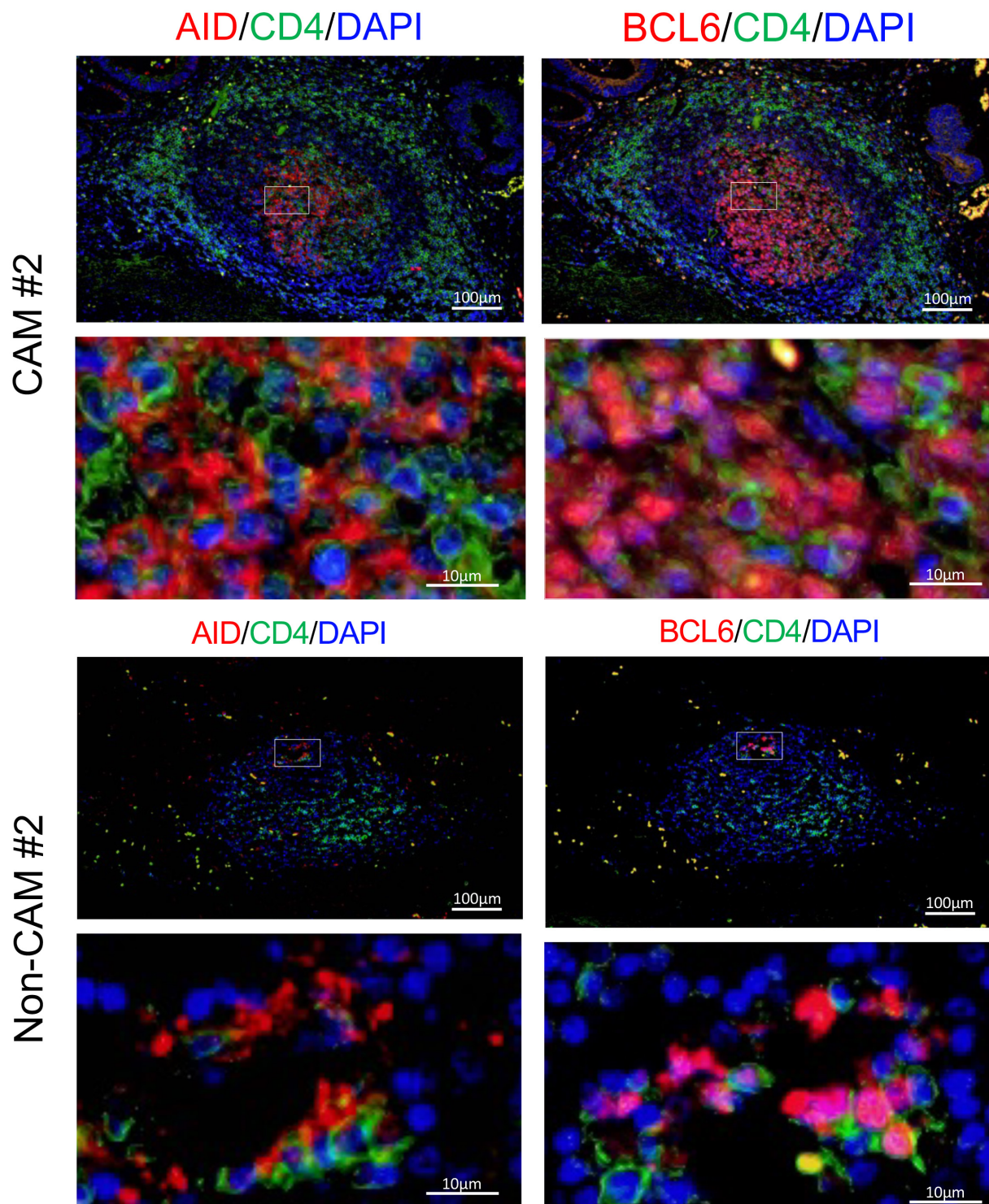


FIGURE 8

CD4⁻AID⁺ class-switched B cells and CD4⁺BCL6⁺ Tfh cells in TLS from a CAM patient and a non-CAM control. Immunofluorescent double-staining of CD4 and AID or BCL6 was conducted using sequential cancer sections. Representative images of the stomach cancer sections obtained from a CAM patient (CAM #2) and a non-CAM control (non-CAM #2) are shown. The staining of AID or BCL6 is shown in red, while CD4 staining is shown in green. Nuclei are counterstained with DAPI (blue). AID and BCL6 were stained in the cytoplasm and nucleus, respectively. The lower panel represents a high magnification image of an inset of the upper panel. Scale bar, 100 µm (upper) and 10 µm (lower). BCL6, B-cell lymphoma 6; TLSs, tertiary lymphoid structures; CAM, cancer-associated myositis; AID, activation induced deaminase; DAPI, 4',6'-diamidino-2'-phenylindole dihydrochloride; Tfh, T follicular helper.

providers that help the organization of GC-like structures via a cognate interaction with B cells, resulting in the promotion of somatic hypermutation and isotypic switching of B cells and the subsequent generation of memory B cells and plasma cells producing high-affinity antibodies (37, 38). Finally, a recent study in patients with ovarian tumors found that TLSs facilitate coordinated antitumor immune responses involving not only high-affinity B cells but also cytolytic CD8⁺ T cells (35). Taken together, similar acquired immune responses might be activated in the primary tumor site in patients with CAM. Effective induction of adaptive immune responses against tumor cells plays a critical role in protection from cancer, while the upregulation of PD-1/PD-L1 plays an important role in evading tumor immune responses (39). Since PD-1/PD-L1 expression levels were positively correlated with expansion of TLSs/TILs in the cancer tissue (40), it is worth assessing a potential relationship between PD-1/PD-L1 expression and development of CAM in future studies.

Interestingly, mutations of genes, such as mismatch repair genes and the B-Raf proto-oncogene, in cancer cells are reported to promote the formation of TLSs (41). Somatic gene mutations and loss of heterozygosity of TIF1- γ , one of the major target autoantigens of CAM-associated MSAs (42), were found more frequently in cancer tissues of CAM patients with anti-TIF1- γ antibody than in those of non-CAM patients without anti-TIF1- γ antibody (43). In addition, it has been reported that the expression of autoantigens targeted by MSAs/MAAs, such as Jo-1 (histidyl-tRNA synthetase), Mi-2, U1-70kD, and Ku, is upregulated in cancer tissue (44). Based on these findings, one can hypothesize that immune responses elicited against self-antigens or modified self-antigens in cancer may be directed to the skin or skeletal muscles, leading to the development of CAM (45), although it was difficult to assess a potential relationship between histological features of TLSs and MSAs in this study due to the small number of patients analyzed.

Recently, much attention has been given to the roles of TLSs detected in the main target organs in the pathogenic process of many autoimmune diseases (46). These include TLSs in the synovium of patients with rheumatoid arthritis (RA), salivary glands of patients with Sjögren's syndrome, and kidneys of patients with systemic lupus erythematosus. Interestingly, the formation of TLSs or TLS-like structures called inducible bronchus-associated lymphoid tissue in the lungs precedes the onset of RA in high-risk subjects who are positive for anti-cyclic citrullinated peptide antibodies (ACPAs) (47). Ectopic production of ACPAs within inducible bronchus-associated lymphoid tissue might be involved in the development of RA through cross-reaction to the citrullinated proteins expressed in the synovium (47, 48). Similarly, adaptive immune responses induced in cancer might cross-react with the autoantigens expressed on the skin and muscles (45). Lymphoid follicular structures similar to TLSs have been reported in the muscle tissue of patients with IIMs (49). It was interesting to compare

TILs and lymphoid follicular structures between the tumor tissue and the affected tissues of CAM, including skeletal muscle and skin, but no case underwent muscle or skin biopsy in this study.

The strength of our study is the comparison between CAM patients and non-CAM patients using the case-control study design, in which background factors known to influence antitumor immune responses in cancer patients were matched between the groups. Another strength was the exclusion of patients who received immunomodulatory treatment before tumor resection surgery. These efforts certainly eliminated the potential influence of heterogeneous cancer factors and immunomodulatory treatment on immunologic features on histology, although major limitations were attributable to this study design. These included a small number of patients subjected to detailed analysis, leading to difficulty in performing appropriate statistical analysis. However, we believe that our findings warrant future studies recruiting a large number of cancer patients with and without CAM to explore a potential interaction between antitumor immunity and autoimmunity that elicits CAM.

Conclusion

The adaptive immune response within TLSs in the primary tumor site might contribute to the development of CAM in selected patients with cancer. Our findings support the potential link between antitumor immunity and autoimmunity.

Data availability statement

The raw data supporting the conclusions of this article will be made available by the authors, without undue reservation.

Ethics statement

The studies involving human participants were reviewed and approved by Institutional Review Board of Nippon Medical School Hospital. The patients/participants provided their written informed consent to participate in this study.

Author contributions

HK, TG, and MK: substantial contributions to the study conception and design, analysis and interpretation of data. HK, TG, SK, YO, MT, MS, and AS: substantial contributions to the acquisition of data. All authors drafting the article or revising it critically for important intellectual content and final approval of the version of the article to be published.

Funding

This work was supported in part by a research grant for Intractable Diseases from the Japanese Ministry of Health, Labour and Welfare (20FC1050) and the Japan Agency for Medical Research and Development (21ek0109531h0001). The funders had no role in the study design, data collection and analysis, decision to publish, or preparation of the manuscript. The Clinical Rebiopsy Bank Project was supported in part by Comprehensive Cancer Therapy Development from the Ministry of Education, Culture, Sports, Science and Technology Supported Program for the Strategic Research Foundation at Private Universities (grant no. S1311022).

Acknowledgments

We are grateful to Professor Hiroshi Yoshida, Professor Toshiyuki Takeshita, and Professor Hiroyuki Takei for providing cancer tissue specimens registered in the Clinical Rebiopsy Bank; Ms. Yuka Okazaki and Yuichiro Shirai for helpful advice; and Zhixing Jiang and Ms. Miyuki Takatori for assisting in the immunohistochemistry analysis.

Conflict of interest

TG received speaking fees from Astellas, Boehringer Ingelheim, Bristol Myers Squibb, Janssen, MBL, Nippon Shinyaku, and Ono Pharmaceuticals. MT received consulting and speaking fees from Amgen, research grants and speaking fee from AbbVie, Asahi Kasei, Chugai, Eisai, and Tanabe-Mitsubishi, and speaking fee from Astellas, Ayumi,

Boehringer Ingelheim, Eli Lilly, Jansen Pharma, Nippon Shinyaku, Novartis, Ono Pharmaceuticals, Takeda, Taisyo, UBC Japan, and Viatrix. MS received the research grants from Chugai, Taiho, Lilly, Boehringer Ingelheim, Nippon Kayaku, and speaking fees from AstraZeneca, Chugai, Taiho, MSD, Lilly, Takeda, Bristol Myers Squibb, Pfizer, Nippon Kayaku, Ono Pharmaceuticals, and Kyowa Kirin Pharmaceuticals. MK holds the patent for the anti-MDA5 antibody measurement kit and received consulting fees, speaking fees, and research grants from AbbVie, Asahi Kasei, Astellas, Boehringer Ingelheim, Chugai, Eisai, Corbus, Kissei, MBL, Mitsubishi Tanabe, Mochida, Nippon Shinyaku, and Ono Pharmaceuticals.

The remaining authors declare that the research was conducted in the absence of any commercial or financial relationships that could be construed as a potential conflict of interest.

Publisher's note

All claims expressed in this article are solely those of the authors and do not necessarily represent those of their affiliated organizations, or those of the publisher, the editors and the reviewers. Any product that may be evaluated in this article, or claim that may be made by its manufacturer, is not guaranteed or endorsed by the publisher.

Supplementary material

The Supplementary Material for this article can be found online at: <https://www.frontiersin.org/articles/10.3389/fmed.2022.1066858/full#supplementary-material>

References

- Lundberg IE, de Visser M, Werth VP. Classification of myositis. *Nat Rev Rheumatol.* (2018) 14:269–78. doi: 10.1038/nrrheum.2018.41
- Thompson C, Piguat V, Choy E. The pathogenesis of dermatomyositis. *Br J Dermatol.* (2018) 179:1256–62. doi: 10.1111/bjd.15607
- Suurmond J, Diamond B. Autoantibodies in systemic autoimmune diseases: specificity and pathogenicity. *J Clin Invest.* (2015) 125:2194–202. doi: 10.1172/JCI78084
- Yang Z, Lin F, Qin B, Liang Y, Zhong R. Polymyositis/dermatomyositis and malignancy risk: a meta-analysis study. *J Rheumatol.* (2015) 42:282–91. doi: 10.3899/jrheum.140566
- Qiang JK, Kim WB, Baibergenova A, Alhusayen R. Risk of malignancy in dermatomyositis and polymyositis: a systematic review and meta-analysis. *J Cutan Med Surg.* (2017) 21:131–6. doi: 10.1177/1203475416665601
- Troyanov Y, Targoff IN, Tremblay JL, Goulet JR, Raymond Y, Sénécal JL. Novel classification of idiopathic inflammatory myopathies based on overlap syndrome features and autoantibodies: analysis of 100 French Canadian patients. *Medicine (Baltimore).* (2005) 84:231–49. doi: 10.1097/01.md.0000173991.74008.b0
- Trallero-Araguas E, Rodrigo-Pendás JA, Selva-O'Callaghan A, Martínez-Gómez X, Bosch X, Labrador-Horrillo M, et al. Usefulness of anti-p155 autoantibody for diagnosing cancer-associated dermatomyositis: a systematic review and meta-analysis. *Arthritis Rheum.* (2012) 64:523–32. doi: 10.1002/art.33379
- Lu X, Peng Q, Wang G. The role of cancer-associated autoantibodies as biomarkers in paraneoplastic myositis syndrome. *Curr Opin Rheumatol.* (2019) 31:643–9. doi: 10.1097/BOR.0000000000000641
- Sharma P, Siddiqui BA, Anandhan S, Yadav SS, Subudhi SK, Gao J. The next decade of immune checkpoint therapy. *Cancer Discov.* (2021) 11:838–57. doi: 10.1158/2159-8290.CD-20-1680
- Paijens ST, Vledder A, de Bruyn M, Nijman HW. Tumor-infiltrating lymphocytes in the immunotherapy era. *Cell Mol Immunol.* (2021) 18:842–59. doi: 10.1038/s41423-020-00565-9
- Gu-Trantien C, Loi S, Garaud S, Equeter C, Libin M, de Wind A, et al. CD4⁺ follicular helper T cell infiltration predicts breast cancer survival. *J Clin Invest.* (2013) 123:2873–92. doi: 10.1172/JCI67428

12. Neyt K, Perros F, GeurtsvanKessel CH, Hammad H, Lambrecht BN. Tertiary lymphoid organs in infection and autoimmunity. *Trends Immunol.* (2012) 33:297–305. doi: 10.1016/j.it.2012.04.006
13. Sautès-Fridman C, Petitprez F, Calderaro J, Fridman WH. Tertiary lymphoid structures in the era of cancer immunotherapy. *Nat Rev Cancer.* (2019) 19:307–25. doi: 10.1038/s41568-019-0144-6
14. Schumacher TN, Thommen DS. Tertiary lymphoid structures in cancer. *Science.* (2022) 375:eabf9419. doi: 10.1126/science.abf9419
15. Lundberg IE, Tjärnlund A, Bottai M, Werth VP, Pilkington C, de Visser M, et al. 2017 European league against rheumatism/American college of rheumatology classification criteria for adult and juvenile idiopathic inflammatory myopathies and their major subgroups. *Arthritis Rheumatol.* (2017) 69:2271–82. doi: 10.1002/art.40320
16. Nakamichi S, Seike M, Miyanaga A, Chiba M, Matsuda K, Kobayashi K, et al. RT-PCR for detecting ALK translocations in cytology samples from lung cancer patients. *Anticancer Res.* (2017) 37:3295–9. doi: 10.21873/anticancer.11696
17. Brierley JD, Gospodarowicz MK, Wittekind C. *TNM Classification of Malignant Tumours*. 8th ed. Hoboken, NJ: Wiley (2017).
18. Kuwana M, Okazaki Y. A multianalyte assay for the detection of dermatomyositis-related autoantibodies based on immunoprecipitation combined with immunoblotting. *Mod Rheumatol.* (2022). [Epub ahead of print]. doi: 10.1093/mr/roac056
19. Hamaguchi Y, Fujimoto M, Matsushita T, Kaji K, Komura K, Hasegawa M, et al. Common and distinct clinical features in adult patients with anti-aminoacyl-tRNA synthetase antibodies: heterogeneity within the syndrome. *PLoS One.* (2013) 8:e60442. doi: 10.1371/journal.pone.0060442
20. Gono T, Okazaki Y, Murakami A, Kuwana M. Improved quantification of a commercial enzyme-linked immunosorbent assay kit for measuring anti-MDA5 antibody. *Mod Rheumatol.* (2019) 29:140–5. doi: 10.1080/14397595.2018.1452179
21. Franco-Iborra S, Tanji K. Histochemical and immunohistochemical staining methods to visualize mitochondrial proteins and activity. *Methods Cell Biol.* (2020) 155:247–70. doi: 10.1016/bs.mcb.2019.11.024
22. Naito Z, Ishiwata T, Kurban G, Teduka K, Kawamoto Y, Kawahara K, et al. Expression and accumulation of lumican protein in uterine cervical cancer cells at the periphery of cancer nests. *Int J Oncol.* (2002) 20:943–8. doi: 10.3892/ijo.20.5.943
23. Yang H, Wei R, Liu Q, Shi Y, Li J. Frequency and distribution of CD4+CXCR5+ follicular B helper T cells within involved tissues in IgG4-related ophthalmic disease. *Mol Med Rep.* (2017) 16:9512–20. doi: 10.3892/mmr.2017.7780
24. Berben L, Wildiers H, Marcellis L, Antoranz A, Bosisio F, Hatse S, et al. Computerised scoring protocol for identification and quantification of different immune cell populations in breast tumour regions by the use of QuPath software. *Histopathology.* (2020) 77:79–91. doi: 10.1111/his.14108
25. Hendry S, Salgado R, Gevaert T, Russell PA, John T, Thapa B, et al. Assessing tumor-infiltrating lymphocytes in solid tumors: a practical review for pathologists and proposal for a standardized method from the international immunooncology biomarkers working group: part 1: assessing the host immune response, TILs in invasive breast carcinoma and ductal carcinoma in situ, metastatic tumor deposits and areas for further research. *Adv Anat Pathol.* (2017) 24:235–51. doi: 10.1097/PAP.0000000000000162
26. Dieu-Nosjean MC, Goc J, Giraldo NA, Sautès-Fridman C, Fridman WH. Tertiary lymphoid structures in cancer and beyond. *Trends Immunol.* (2014) 35:571–80. doi: 10.1016/j.it.2014.09.006
27. Engelhard VH, Rodriguez AB, Mauldin IS, Woods AN, Peske JD, Slingluff CL Jr. Immune cell infiltration and tertiary lymphoid structures as determinants of antitumor immunity. *J Immunol.* (2018) 200:432–42. doi: 10.4049/jimmunol.1701269
28. Klein C, Devi-Marulkar P, Dieu-Nosjean MC, Germain C. Development of tools for the selective visualization and quantification of TLS-immune cells on tissue sections. *Methods Mol Biol.* (2018) 1845:47–69. doi: 10.1007/978-1-4939-8709-2_4
29. Fridman WH, Meylan M, Petitprez F, Sun CM, Italiano A, Sautès-Fridman C. B cells and tertiary lymphoid structures as determinants of tumour immune contexture and clinical outcome. *Nat Rev Clin Oncol.* (2022) 19:441–57. doi: 10.1038/s41571-022-00619-z
30. Munoz-Erazo L, Rhodes JL, Marion VC, Kemp RA. Tertiary lymphoid structures in cancer - considerations for patient prognosis. *Cell Mol Immunol.* (2020) 17:570–5. doi: 10.1038/s41423-020-0457-0
31. Jacquelot N, Tellier J, Nutt SL, Belz GT. Tertiary lymphoid structures and B lymphocytes in cancer prognosis and response to immunotherapies. *Oncoimmunology.* (2021) 10:1900508. doi: 10.1080/2162402X.2021.1900508
32. Li H, Wang J, Liu H, Lan T, Xu L, Wang G, et al. Existence of intratumoral tertiary lymphoid structures is associated with immune cells infiltration and predicts better prognosis in early-stage hepatocellular carcinoma. *Aging (Albany NY).* (2020) 12:3451–72. doi: 10.18632/aging.102821
33. Li H, Liu H, Fu H, Li J, Xu L, Wang G, et al. Peritumoral tertiary lymphoid structures correlate with protective immunity and improved prognosis in patients with hepatocellular carcinoma. *Front Immunol.* (2021) 12:648812. doi: 10.3389/fimmu.2021.648812
34. Hiraoka N, Ino Y, Yamazaki-Itoh R. Tertiary lymphoid organs in cancer tissues. *Front Immunol.* (2016) 7:244. doi: 10.3389/fimmu.2016.00244
35. Kroeger DR, Milne K, Nelson BH. Tumor-infiltrating plasma cells are associated with tertiary lymphoid structures, cytolytic T-cell responses, and superior prognosis in ovarian cancer. *Clin Cancer Res.* (2016) 22:3005–15. doi: 10.1158/1078-0432.CCR-15-2762
36. Helmink BA, Reddy SM, Gao J, Zhang S, Basar R, Thakur R, et al. B cells and tertiary lymphoid structures promote immunotherapy response. *Nature.* (2020) 577:549–55. doi: 10.1038/s41586-019-1922-8
37. Hetta HF, Elkady A, Yahia R, Meshall AK, Saad MM, Mekky MA, et al. T follicular helper and T follicular regulatory cells in colorectal cancer: a complex interplay. *J Immunol Methods.* (2020) 480:112753. doi: 10.1016/j.jim.2020.112753
38. Gu-Trantien C, Migliori E, Buisseret L, de Wind A, Brohée S, Garaud S, et al. CXCL13-producing Th cells link immune suppression and adaptive memory in human breast cancer. *JCI Insight.* (2017) 2:e91487. doi: 10.1172/jci.insight.91487
39. Shan J, Han D, Shen C, Lei Q, Zhang Y. Mechanism and strategies of immunotherapy resistance in colorectal cancer. *Front Immunol.* (2022) 13:1016646. doi: 10.3389/fimmu.2022.1016646
40. Buisseret L, Garaud S, de Wind A, Van den Eynden G, Boisson A, Solinas C, et al. Tumor-infiltrating lymphocyte composition, organization and PD-1/ PD-L1 expression are linked in breast cancer. *Oncoimmunology.* (2016) 6:e1257452. doi: 10.1080/2162402X.2016.1257452
41. Posch F, Silina K, Leibl S, Mündlein A, Moch H, Siebenhüner A, et al. Maturation of tertiary lymphoid structures and recurrence of stage II and III colorectal cancer. *Oncoimmunology.* (2017) 7:e1378844. doi: 10.1080/2162402X.2017.1378844
42. Best M, Molinari N, Chasset F, Vincent T, Cordel N, Bessis D. Use of anti-transcriptional intermediary factor-1 gamma autoantibody in identifying adult dermatomyositis patients with cancer: a systematic review and meta-analysis. *Acta Derm Venereol.* (2019) 99:256–62. doi: 10.2340/00015555-3091
43. Pinal-Fernandez I, Ferrer-Fabregas B, Trallero-Araguas E, Balada E, Martinez MA, Milisenda JC, et al. Tumor TIF1 mutations and loss of heterozygosity related to cancer-associated myositis. *Rheumatology (Oxford).* (2018) 57:388–96. doi: 10.1093/rheumatology/kex413
44. Casciola-Rosen L, Nagaraju K, Plotz P, Wang K, Levine S, Gabrielson E, et al. Enhanced autoantigen expression in regenerating muscle cells in idiopathic inflammatory myopathy. *J Exp Med.* (2005) 201:591–601. doi: 10.1084/jem.20041367
45. De Vooght J, Vulsteke JB, De Haes P, Bossuyt X, Lories R, De Langhe E. Anti-TIF1-γ autoantibodies: warning lights of a tumour autoantigen. *Rheumatology (Oxford).* (2020) 59:469–77. doi: 10.1093/rheumatology/kez572
46. Bombardieri M, Lewis M, Pitzalis C. Ectopic lymphoid neogenesis in rheumatic autoimmune diseases. *Nat Rev Rheumatol.* (2017) 13:141–54. doi: 10.1038/nrrheum.2016.217
47. Sigaux J, Biton J, André E, Semerano L, Boissier MC. Air pollution as a determinant of rheumatoid arthritis. *Joint Bone Spine.* (2019) 86:37–42. doi: 10.1016/j.jbspin.2018.03.001
48. Rangel-Moreno J, Hartson L, Navarro C, Gaxiola M, Selman M, Randall TD. Inducible bronchus-associated lymphoid tissue (iBALT) in patients with pulmonary complications of rheumatoid arthritis. *J Clin Invest.* (2006) 116:3183–94. doi: 10.1172/JCI28756
49. Radke J, Koll R, Preuße C, Pehl D, Todorova K, Schönemann C, et al. Architectural B-cell organization in skeletal muscle identifies subtypes of dermatomyositis. *Neurol Neuroimmunol Neuroinflamm.* (2018) 5:e451. doi: 10.1212/NXI.0000000000000451